Electronic Supplementary Material (ESI) for Journal of Materials Chemistry C.

Supporting Information

Deciphering the Behavior of a New MOF and its Composites Under Light at Ensemble and Single Crystal Levels: Relevance to its Photonic Applications

Eduardo Gomez,[a] Daisuke Yasumiya,[b] Norimitsu Tohnai,[b] Miquel Moreno[c], Boiko Cohen,*[a] Ichiro Hisaki*[d] and Abderrazzak Douhal*[a]

[a] Departamento de Química Física, Facultad de Ciencias Ambientales y Bioquímica, and INAMOL, Universidad de Castilla-La Mancha, Avenida Carlos III, S.N., 45071 Toledo, Spain.

[b] Graduate School of Engineering, Osaka University, 2-1 Yamadaoka, Suita, Osaka 565-0871, Japan.

[c] Departament de Química, Universitat Autónoma de Barcelona, Ballaterra, 08193 Barcelona, Spain.

[d] Graduate School of Engineering Science, Osaka University, 1-3 Machikaneyama, Toyonaka, Osaka 560-8531, Japan.

*Corresponding authors: E-mail address: boyko.koen@uclm.es, hisaki@chem.es.osaka-u.ac.jp and abderrazzak.douhal@uclm.es

1. General

^{1}H and ^{13}C NMR spectra were measured by a JEOL or Bruker spectrometer (400 or 600 MHz for ^{1}H and 100 or 150 MHz for ^{13}C). Mass spectrum data were obtained from a JEOL JMS-700 instrument or autoflex III Bruker. Thermo gravimetric (TG) analyses were performed on Rigaku instruments RIGAKU TG-DTA 8120 under an N_2 purge at a heating rate of 10 °C min^{-1}.

X-Ray diffraction measurements: Powder X-ray diffraction data were collected on a Rigaku Rint-Ultima III diffractometer using graphite-monochromatized Cu-Kα radiation (λ = 1.54187 Å) at room temperature. **Single crystal diffraction:** Diffraction data were collected at 100 K on a DECTRIS EIGER X 1M diffractometer with Si (111) mono-chromated synchrotron radiation (l= 0.81089 Å) at BL40XU (SPring-8)[S3] Direct methods (SHELXT) were used for the structure solution of the crystals. All calculations were performed with the observed reflections [I >2σ(I)] with the program CrystalStructure crystallographic software packages,[1] except for refinement, which was performed using SHELXL.[2, 3] All non-hydrogen atoms were refined with anisotropic displacement parameters, and hydrogen atoms were placed in idealized positions and refined as rigid atoms with the isotropic displacement parameters.

Picosecond-time resolved fluorescence experiments using a TCSPC: Picosecond (ps) emission decays were measured using a time-correlated single photon counting (TCSPC) system.[4] For the excitation at 371, 390 and 635 nm, the samples were excited by a 40-ps pulsed diode laser (<5 mW, 40 MHz repetition rate) and the instrument response function (IRF) was ~ 70 ps. For the excitation at 510 nm we used the second harmonic from the output (1020 nm) of a Ti:sapphire oscillator (Mai Tai HP, Spectra Physics, 90 fs, 250 mW, 80 MHz). In this experiment, the instrument response function (IRF) was ~ 50 ps, and the femtosecond-laser excitation was set at low power (~ 3 mW) to avoid undesired photochemistry. The IRF of the system for solution samples was measured using a standard LUDOX (Sigma-Aldrich) suspension in a 1-cm cell, while for solid state samples, the IRF was measured using portion of the reflected laser.

Time-resolved FLIM experiments: The fluorescence lifetime imaging (FLIM) measurements were performed on a MicroTime 200 confocal microscope (PicoQuant). As an excitation source, we used a diode laser with an excitation wavelength of 390 nm (40 ps full width at half-maximum of intensity). Briefly, it consists of inverse Olympus IX 71 microscope equipped with a water immersion objective (x60 NA1.2, Olympus) and 2D piezo scanner (Physik Instrumente). The emitted light is then focused on a 50-μm pinhole and later collimated to two independent single photon avalanche photodiodes (Micro-Photon-Devices) for time-resolved measurements. The emission spectra were collected through Shamrock SR-303i (Andor Technology) imaging spectrograph and detected by Andor Newton EMCCD camera (Andor Technology). For the anisotropy measurements the light was passed through a polarizing beam-splitter that allows for the simultaneous detection of the parallel and perpendicular parts of the emission. A G-factor of 1.2, accounting for differences in the detection sensitivity for both polarizations in the setup, was used in the calculation of the anisotropy. To calculate the histogram of anisotropy, we used the SymPhoTime Analysis program (PicoQuant), which calculates the static anisotropy on an image.[5] The limits for the anisotropy are -0.5 to 1.0 (-0.5 corresponds to perpendicular orientation and 1.0 to parallel).[6] The emission spectra were collected using one long pass filters (HQ430LP Chroma), while the emission decays were collected using different type of filters depending on the interrogated region (FF01-445-40-25, FF01-503-40-25, FF01-623-32-25 and FF01-650-54-25 BrightLine® filters (Semrock)).

Theoretical calculations

The theoretical calculations have been performed at the DFT level. In order to prevent the well-known problem of excited states with internal charge transfer character the long-range corrected hybrid functional CAM-B3LYP[7] has been used with the 6-31G(d,p) basis set.[8, 9] The excited electronic states have been obtained within the linear Time Dependent-DFT (TDDFT) formalism. Full optimization of the different states has been carried without any symmetry restriction. The solvent effect (Dimethylformamide) has been introduced through the self-consistent PCM continuum method that defines a cavity of solvent (with a specific dielectric constant) where the molecule (solute) is introduced. Polarization of the molecule by the surrounding solvent is accounted for the self-consistent procedure.[10, 11] All calculations have been carried out using the Gaussian09 suite of programs.[12]

2. Synthesis of isoT12H$_6$

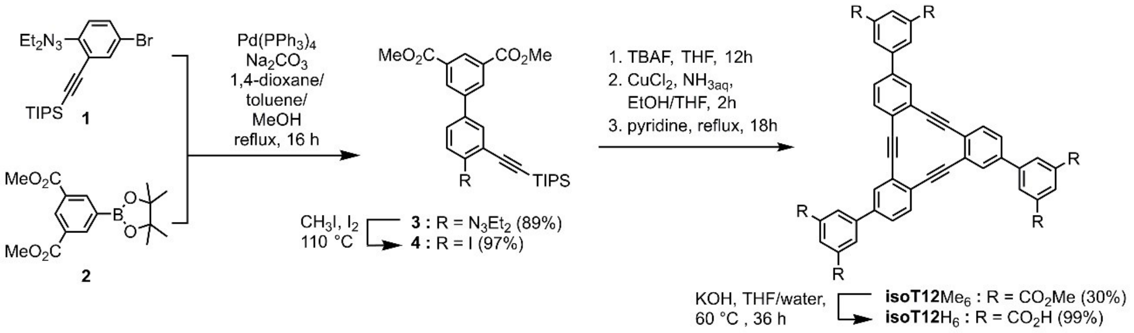

Scheme S1. Synthesis of ligand **isoT12**H$_6$.

Biphenyl derivative 3. Under a nitrogen atmosphere, a suspension of bromobenzene derivative **1** (6.00 g, 13.7 mmol), dimethyl isophthalate **2** (6.40 g, 20.0 mmol), Pd(PPh$_3$)$_4$

(780 mg, 0.675 mmol), Na_2CO_3 (3.40 g, 32.1 mmol) in a degassed mixture of dioxane (50 mL), toluene (50 mL), and methanol (50 mL) was stirred for 16 h under a reflux condition. The solvent was removed in vacuo and reaction mixture was extracted with CH_2Cl_2, washed with water and brine, dried over anhydrous $MgSO_4$. The product was purified by column chromatography (silica gel, Hexane/CH_2Cl_2 = 8/2 to 6/4) to give **3** (6.69 g, 89%) as an orange viscous material.

3: ^{1}H NMR (600 Hz, $CDCl_3$) δ 8.62 (t, J = 1.8, Hz, 1H, ArH), 8.44 (d, J = 1.8 Hz, 2H, ArH), 7.75 (d, J = 2.4 Hz, 1H, ArH), 7.56 (d, J = 8.4 Hz, 1H, ArH), 7.52 (dd, J = 2.4, 8.4 Hz, 1H, ArH), 3.98 (s, 6H, -OCH_3), 3.84 (br, 4H, CH_2CH$_3$), 1.35 (br, 3H, CH$_2$CH_3), 1.26 (br, 3H, CH$_2$CH_3), 1.16 (s, 18H+3H, CH(CH_3)$_2$) ppm. ^{13}C NMR (150 MHz, $CDCl_3$) δ 166.3, 152.5, 141.2, 135.1, 132.3, 132.0, 131.1, 129.0, 127.7, 119.1, 117.3, 105.0, 94.7, 52.5, 49.0, 41.4, 18.8, 11.4 ppm. HRMS (EI): *m/z* calcd. for $[M]^+$ $C_{31}H_{43}N_3O_4Si$: 549.3023; found: 549.3020.

Iodobenzene derivative 4. A solution of triazene derivative **3** (6.69 g, 12.2 mmol) and iodine (50 mg,) dissolved in CH_3I (400 mL) was divided into five potions, each of which was placed in a pressure glass bottle and stirred for 24 h at 110 °C. After the solvent was replaced in vacuo, the reaction mixture was extracted by CH_2Cl_2, washed with aqueous $Na_2S_2O_3$, water, and brine, and dried over anhydrous $MgSO_4$. The product was purified by column chromatography (silica gel, CH_2Cl_2) to give **4** (6.77 g, 97%) as a pale yellow viscous material, which gradually turned into a crystalline solid.

4: mp. 94.0 °C. ^{1}H NMR (600Hz, $CDCl_3$) δ 8.67 (t, J = 1.8 Hz, 1H, ArH), 8.41 (d, J = 1.8 Hz, 2H, ArH), 7.94 (d, J = 8.4 Hz, 1H, ArH), 7.73 (d, J = 1.8 Hz, 1H, ArH), 7.26 (dd, J = 1.8, 8.4 Hz, 1H, ArH), 3.99 (s, 6H, -OCH_3), 1.19 (s, 18H, CH(CH_3)$_2$), 1.18 (s, 3H, CH(CH$_3$)$_2$) ppm. ^{13}C NMR (150 MHz, $CDCl_3$) δ 166.1, 140.3, 139.4, 138.9, 132.1, 131.5, 131.4, 130.9, 129.9, 128.1, 107.6, 100.9, 96.3, 52.6, 18.8, 11.4 ppm. HRMS (EI): *m/z* calcd. for $[M]^+$ $C_{27}H_{33}IO_4Si$: 576.1193; found: 576.1191.

isoT12Me$_6$. A 1M solution of tetrabutylammonium fluoride (12.0 mL, 12.0 mmol) was added dropwise into a solution of triisopropylsilylethynylbenzene derivative **4** (6.77 g, 11.7 mmol) dissolved in wet THF (150 mL). After stirred for 12 h at room temperature, the product was extracted by chloroform, washed with water and brine, and dried over anhydrous $MgSO_4$, to give burgundy oil. The product was passed through a bed of silica gel to afford desilylated precursor as a right brown solid, which was used in the next step without further purification.

A solution of the precursor dissolved in THF (35 mL) was diluted with EtOH (230 mL) and added dropwise into a 25% aqueous NH_3 solution (300 mL) in an ice bath. The reaction mixture was stirred for 2 h at the temperature. Resultant precipitate was filtered, washed with water, and well dried in vacuo to give copper acetylide as a yellow solid. The suspension of the copper acetylide in pyridine (450 mL) and refluxed under a nitrogen atmosphere for 18 h. After removing pyridine in vacuo, the product was purified by column chromatography (silica gel, CH_2Cl_2 to $CHCl_3$) and rinsed with CH_2Cl_2 to give **isoT12**Me_6 (1.02 g, 30% from **4**) as a yellow solid.

isoT12Me_6**:** mp. (dec.) 340 °C. ^1H NMR (600Hz, $CDCl_3$) δ 8.68 (t, J = 1.8 Hz, 3H, ArH), 8.47 (d, J = 1.2 Hz, 6H, ArH), 7.71 (d, J = 1.8 Hz, 3H, ArH), 7.55 (dd, J = 1.8, 8.4 Hz, 3H, ArH), 7.52 (d, J = 7.8 Hz, 3H, ArH), 4.00 (s, 18H, $-OCH_3$) ppm. ^{13}C NMR (150 MHz, $CDCl_3$, 50 °C) δ 166.0, 140.2, 139.4, 132.8, 131.9, 131.6, 130.7, 130.1, 127.7, 127.3, 126.5, 93.9, 93.2, 52.5 ppm. HRMS (FAB): *m/z* calcd. for $[M]^+$ $C_{54}H_{36}O_{12}$: 876.2207; found: 876.2231.

isoT12$\mathbf{H_6}$**.** A suspension of isoT12Me_6 (1.02 g, 1.16 mmol) and KOH (586 mg, 10.4 mmol) in THF (130 mL)/ water (70 mL) was stirred at 60 °C for 36 h. The suspension gradually turned to a clear yellow solution. The reaction mixture was passed through a filter paper, and the filtrate was acidified by adding aqueous HCl dropwise. The yellow precipitate was filtered and washed with water to give isoT12H_6 (915 mg, 99%) as a brown-yellow solid.

isoT12H_6**:** mp. (dec) 245 °C. ^1H NMR (600Hz, DMSO-d_6) δ 8.50 (t, J = 1.2 Hz, 3H, ArH), 8.42 (d, J = 1.2 Hz, 6H, ArH), 7.84 (d, J = 1.8 Hz, 3H, ArH), 7.75 (dd, J = 1.8, 8.4 Hz, 3H, ArH), 7.67 (d, J = 7.8 Hz, 3H, ArH) ppm. ^{13}C NMR (150 MHz, DMSO-d_6, 80 °C) δ 165.9, 138.9, 138.7, 132.7, 132.1, 130.6, 129.8, 129.1, 127.4, 126.3, 125.0, 93.2, 92.5 ppm. HRMS (EIS): *m/z* calcd. for $[M-H]^-$ $C_{48}H_{23}O_{12}$: 791.1195; found: 791.1222.

MOF-isoT12(Zn). To a solution of $Zn(NO_3)_2{\bullet}6H_2O$ (37.5 mg, 0.126 mmol, 10 eq.) dissolved in DMF (1mL) was added a solution of isoT12H_6 (10.0 mg, 0.0126 mmol) dissolved in DMF (2 mL). The mixed solution in a sample tube sealed with a cap was placed in thermostatic oven at 80 °C for 1 day to give MOF-isoT12(Zn) (15.4 mg) as a yellow-orange crystalline precipitate. Notably, when 60 equivalents of Zn(II) were used for the MOF preparation (namely in the case of MOF-isoT12(Zn)-60), both A- and B-sites are bridged by the zinc formate with occupancies of 0.5 and 0.7, respectively. Because of the bridging at the B-site, the crystallographic c axis of MOF-isoT12(Zn)-60 was shortened by 0.39 Å. These bridges also play a role to fill gaps among the T12 panels (Figure S3). Anal. Calc. For $(\mathrm{isoT12})\cdot\mathrm{Zn_3}\cdot(\mathrm{H_2O})_2\cdot(\mathrm{2DMF})_{0.7}\cdot[\mathrm{OCHOZn(DMF)_4OCHO}]_{0.3}\cdot3[\mathrm{Zn(NO_3)_2}\cdot6(\mathrm{H_2O})]$ C 49.1, H 5.66, N 9.07, residual 36.08%. Found: C 49.50, H 5.47, N 8.86, residual 36.17.

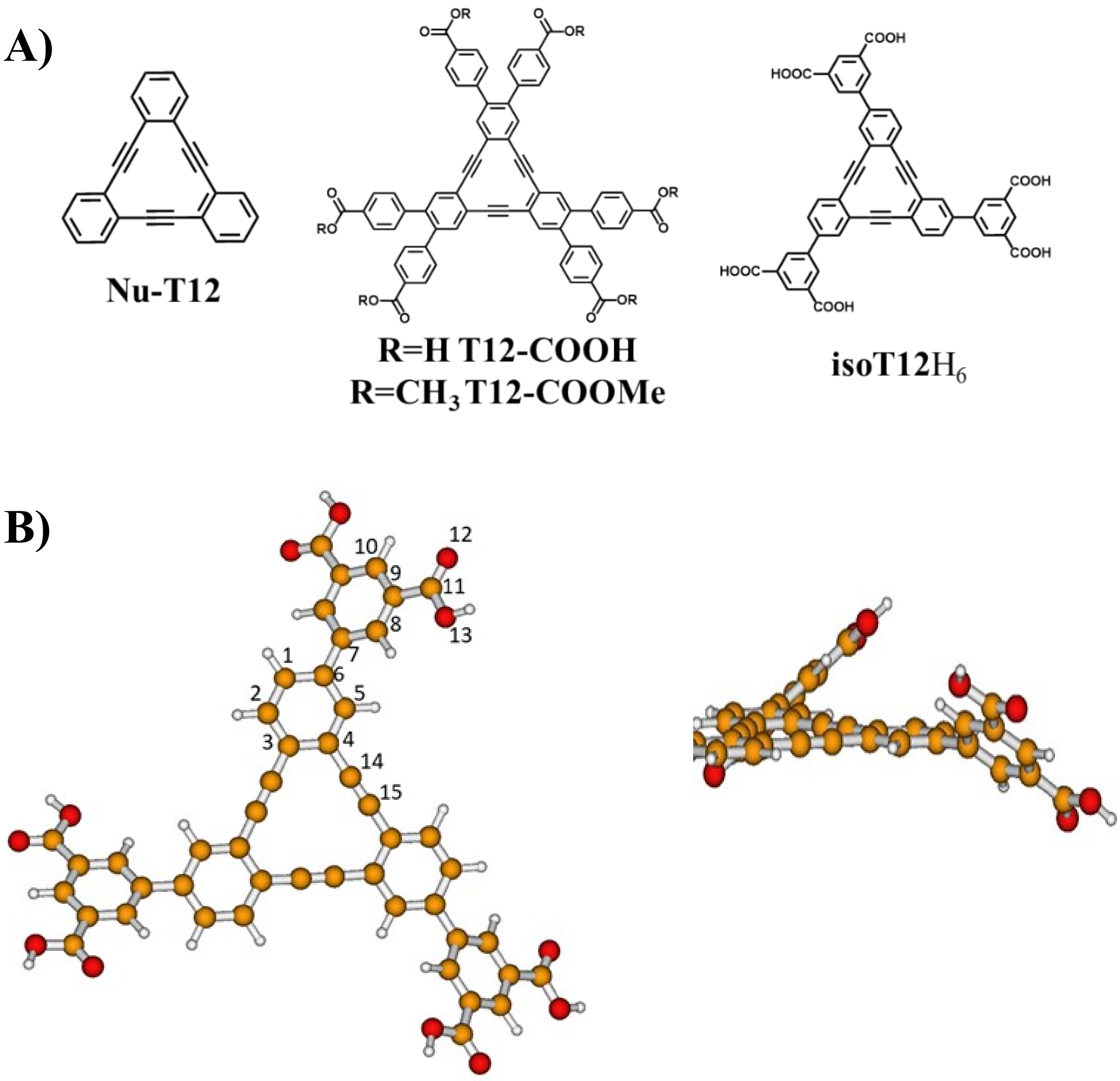

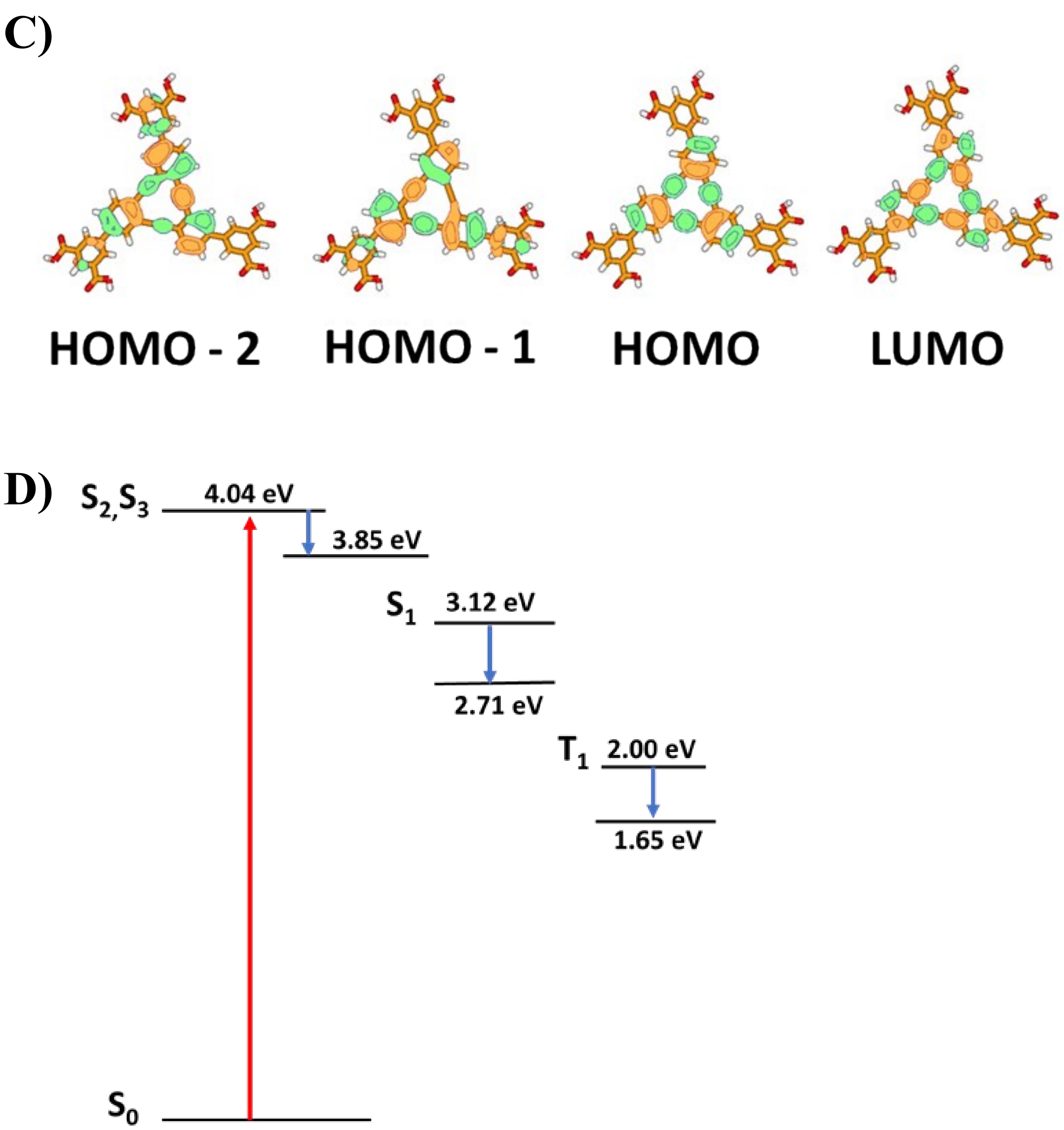
C)
HOMO - 2
HOMO - 1
HOMO
LUMO
D)
S_2,S_3
4.04 eV
3.85 eV
S_1
3.12 eV
2.71 eV
T_1
2.00 eV
1.65 eV
S_0

E)

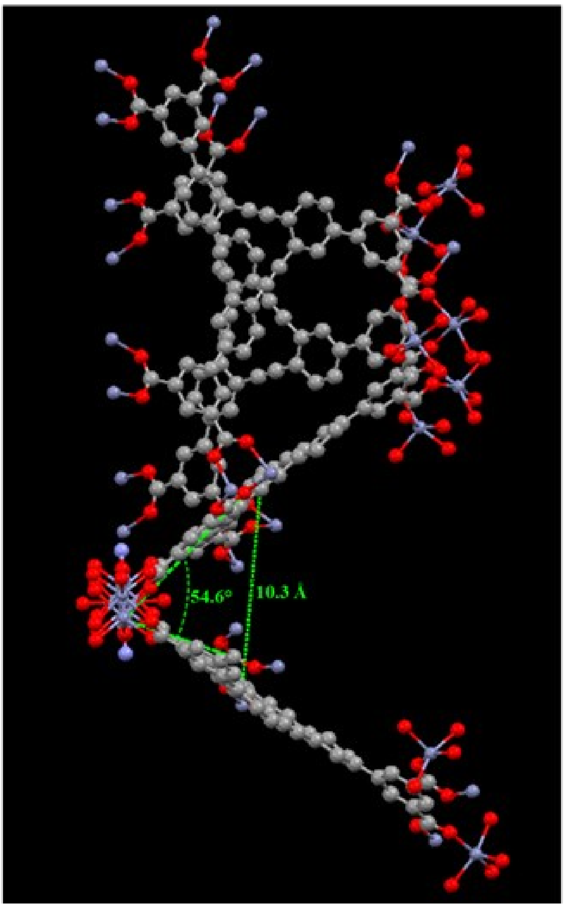

Scheme S2. A) Chemical structures of Nu-T12, T12-COOH, T12-COOMe and isoT12H_6. B) Predicted most stable conformation of isoT12H_6 in presence DMF. C) Frontier molecular orbitals involved in the electronic states of isoT12H_6. The numeration of the C atoms used in Table S2 are shown in Scheme S2B. D) Schematic representation of the energy levels of the different electronic states (not in scale) of isoT12H_6 in DMF solution. The horizontal lines give the energy level of each state at its optimized geometry. The red arrow represents the vertical excitation from the ground state. The blue arrows correspond to geometry relaxations within the same electronic state from the Franck-Condon (FC) geometry to the relaxed one. E) Structure of the MOF-isoT12(Zn) showing the angle and the distance between two neighboring ligands.

3. Crystallographic analysis

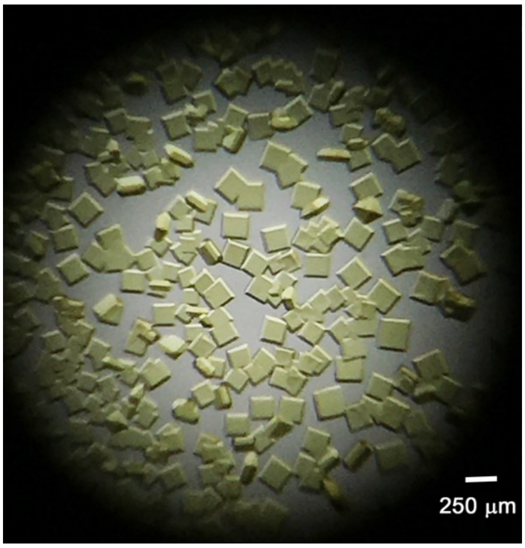

Figure S1. Optical microscope image of MOF-isoT12(Zn) crystals.

	MOF-isoT12(Zn)
Formula	$(C_{48}H_{18}O_{12})Zn_3O_3$ $(C_{0.15}H_{0.15}O_{0.44}Zn_{0.07})$ [+solvent]
Fw	1044.67
System	tetragonal
Space group	$I4/m$ (no.87)
a	30.86932(9)
b	30.86932(9)
c	46.7574(2)
α	90
β	90
γ	90
V	44555.8(3)
***Temp* / K**	100
Z	16
Reflns obs / unique	281851 / 27514
***R*1**	0.0567
***wR*(all)**	0.1905
CCDC	2043938

Table S1. Crystal structure data of MOF-isoT12(Zn).

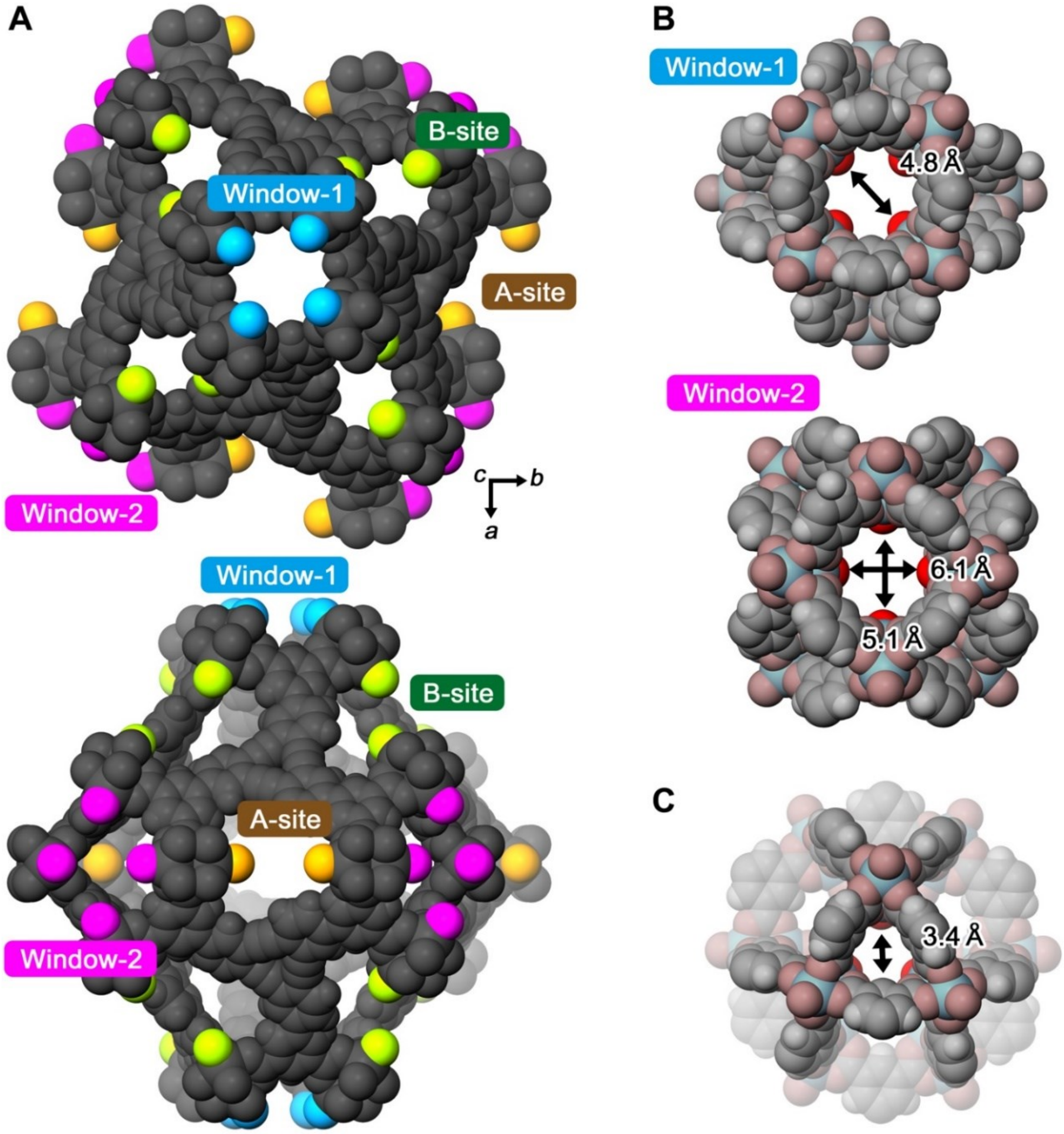

Figure S2. Representation of the location and sizes of windows and additional coordination sites in the MOF-isoT12(Zn) framework. A) Location of A- and B-sites, and windows -1 and -2. B) Dimensions of windows-1 and -2. C) A small window located between the spherical and tetrahedral spaces. A-sites are partly occupied by zinc formate bridge with occupancy of 0.3, while B-sites are not.

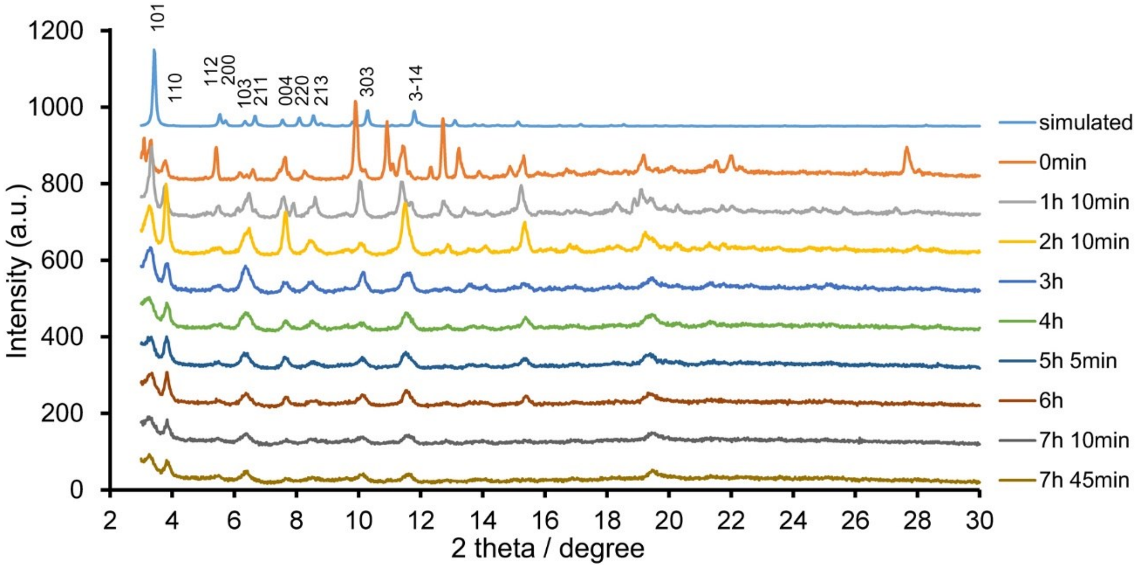

Figure S3. Powder X-ray diffraction (PXRD) patterns of MOFs-isoT12(Zn) collected at different times (as indicated). The loss of crystallinity is due a desolvation (removal of DMF molecules) of the crystals.

4. Thermogravimetric analysis

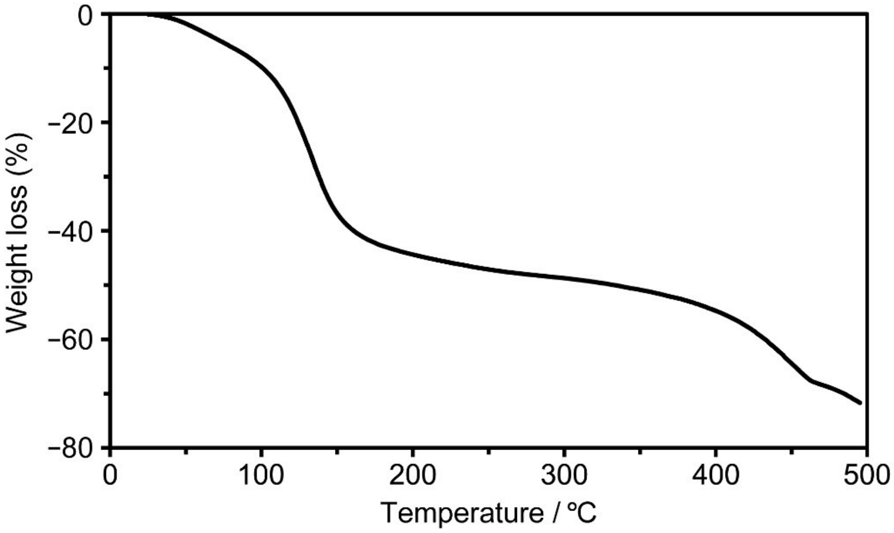

Figure S4. Thermogravimetric (TG) analysis of MOFs-isoT12(Zn).

5. NMR spectra of synthesized compounds

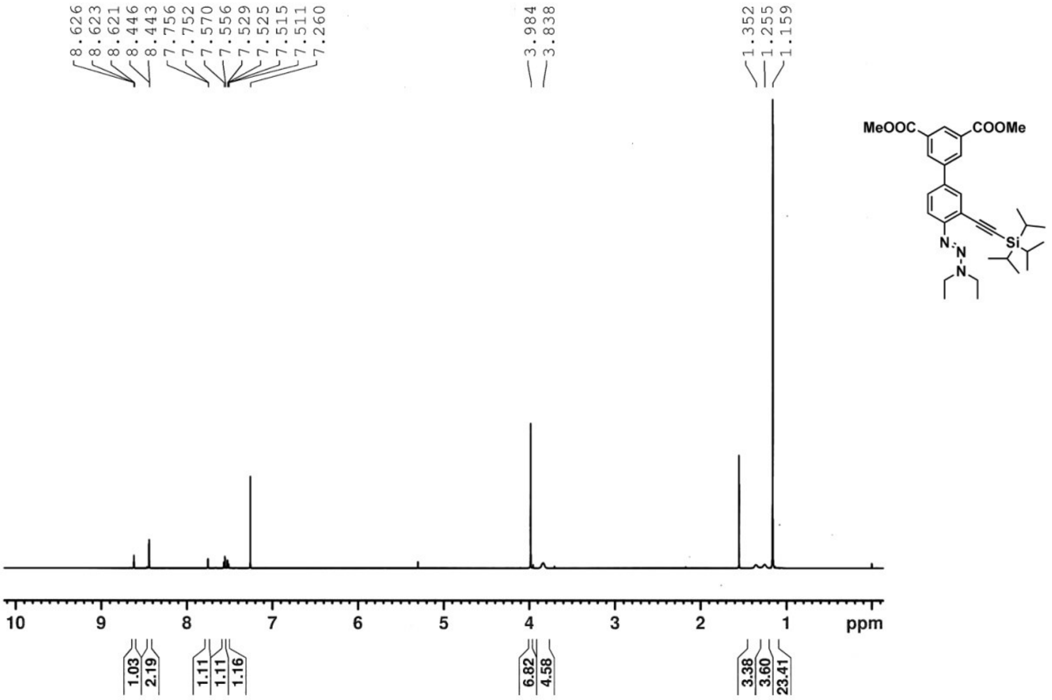

Figure S5. ^{1}H NMR (600 MHz, in CDCl$_3$) spectrum of triazene derivative **3.**

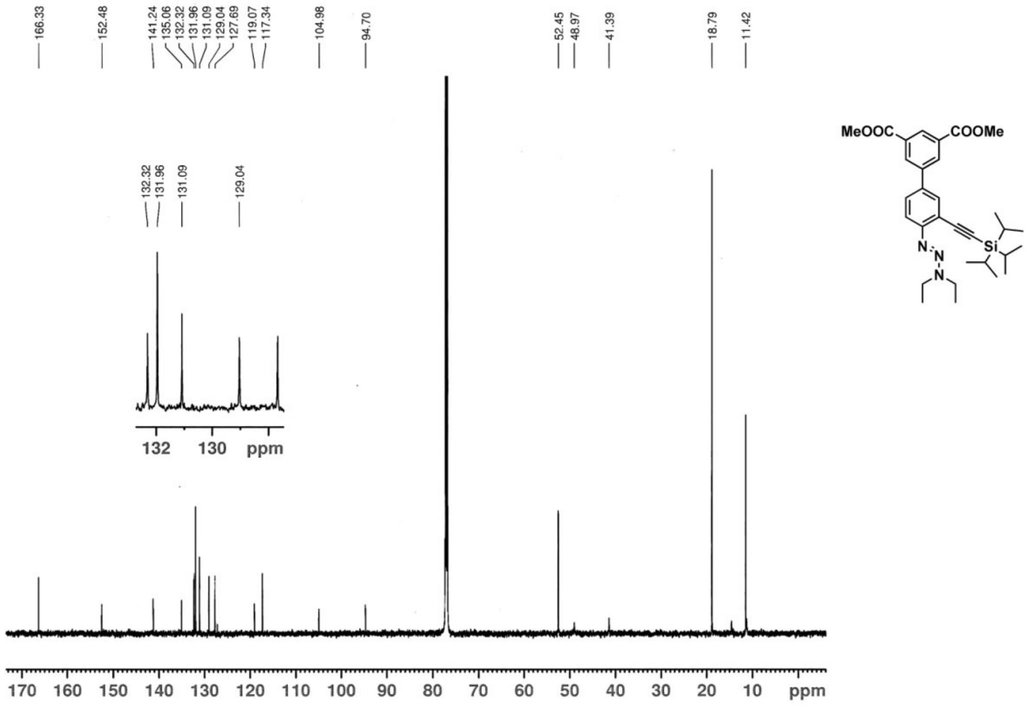

Figure S6. ^{13}C NMR (150 MHz, in CDCl$_3$) spectrum of triazene derivative **3.**

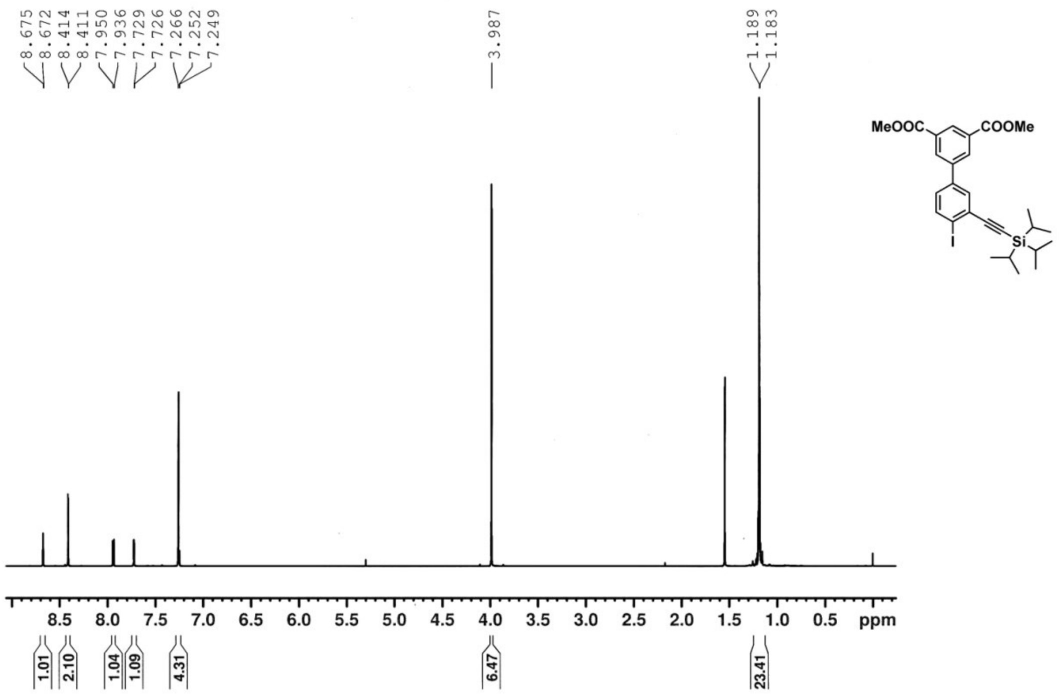

Figure S7. ^{1}H NMR (600 MHz, in CDCl$_3$) spectrum of iodobenzene derivative **4.**

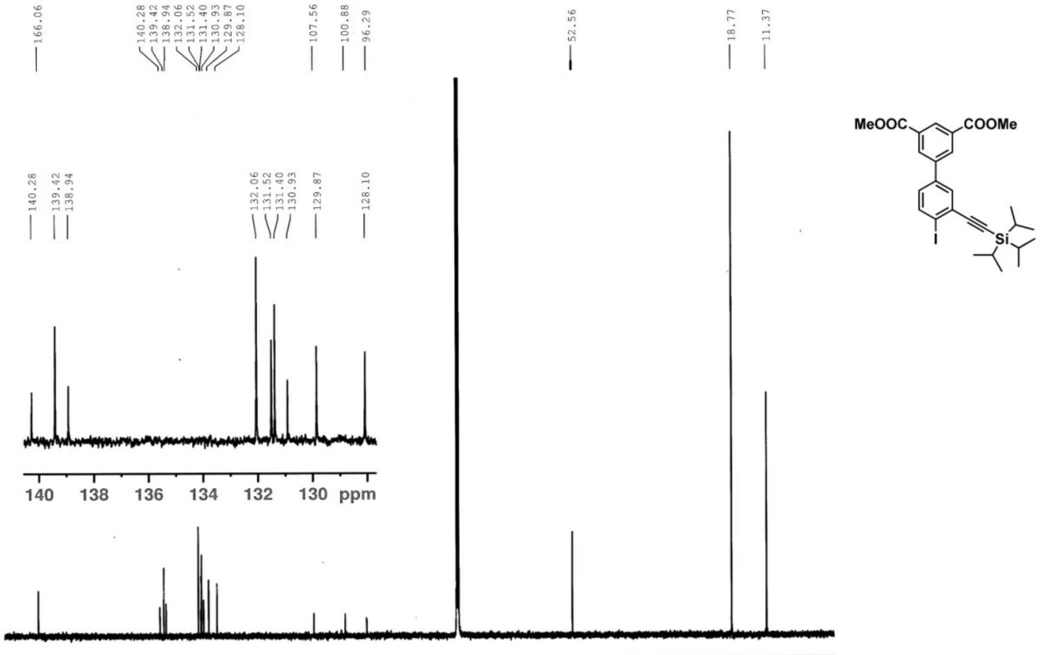

Figure S8. ^{13}C NMR (150 MHz, in CDCl$_3$) spectrum of iodobenzene derivative **4.**

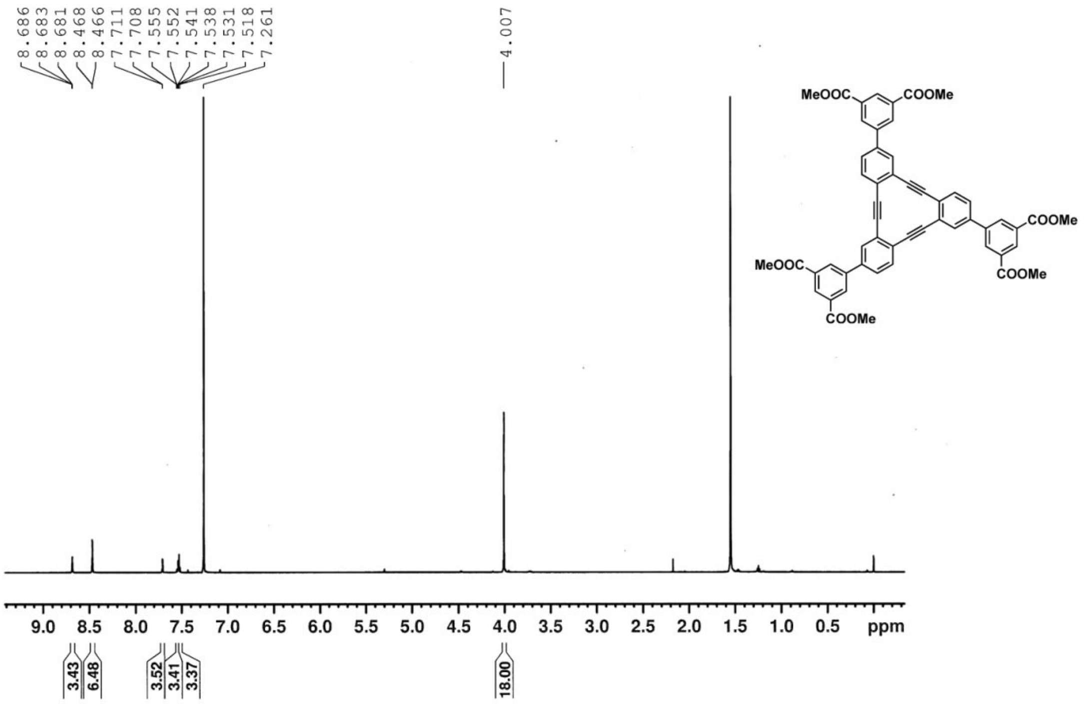

Figure S9. ^{1}H NMR (600 MHz, in $CDCl_3$) spectrum of isoT12Me$_6$.

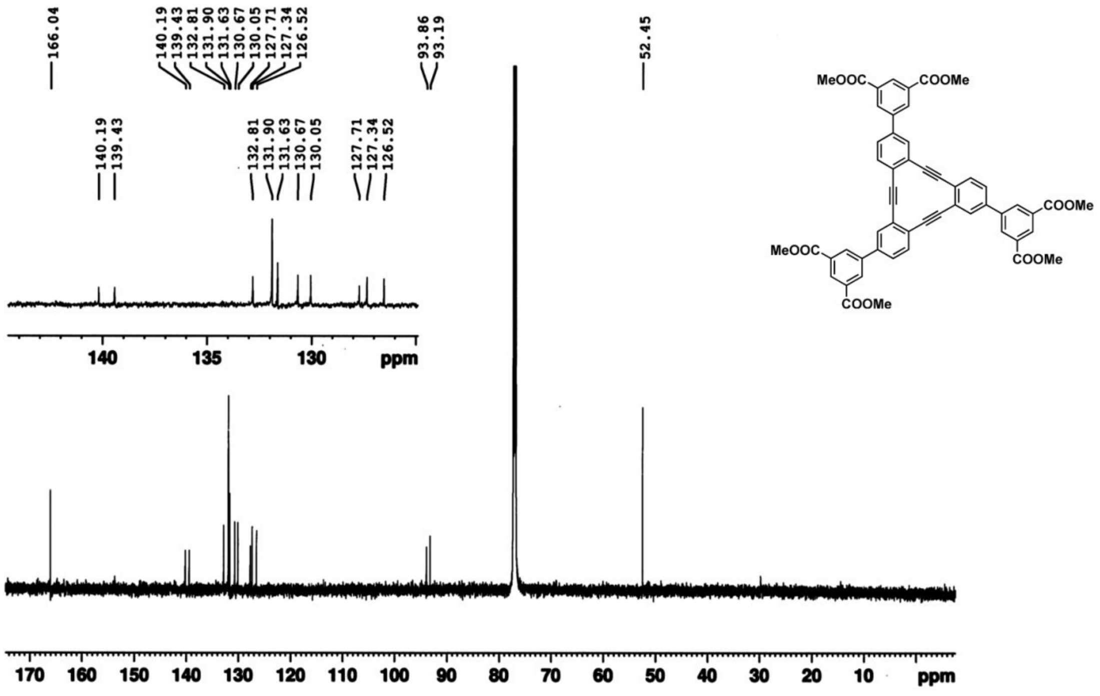

Figure S10. ^{1}H NMR (150 MHz, in $CDCl_3$, 50 °C) spectrum of isoT12Me$_6$.

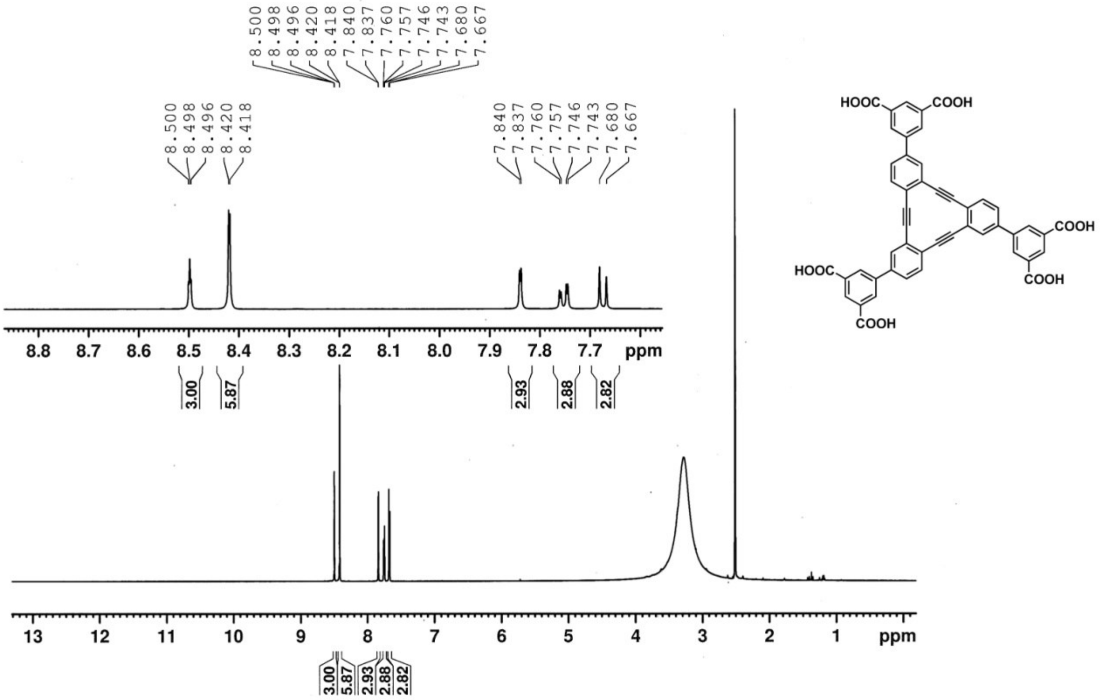

Figure S11. ^1H NMR (150 MHz, in DMSO-d_6) spectrum of isoT12H$_6$.

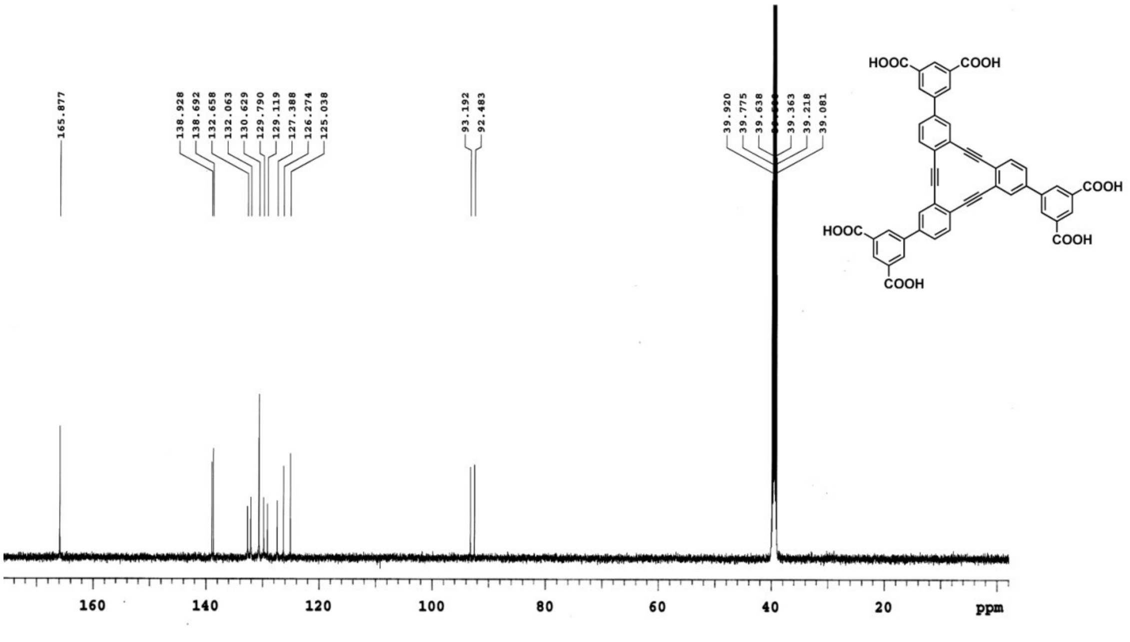

Figure S12. ^{13}C NMR (150 MHz, in DMSO-d_6, 80 °C) spectrum **MOF-isoT12(Zn)**

6. Data from theoretical calculations

Table S2A

Atom	S_0	S_1(FC)	S_1	S_2(FC)	S_2	T_1(FC)	T_1
1	-0.002	-0.007	-0.003	-0.008	-0.008	-0.005	-0.002
2	0.021	0.025	0.032	0.016	0.016	0.022	0.029
3	0.020	0.010	-0.037	0.015	0.015	0.016	-0.033
4	0.032	0.022	-0.019	0.023	0.023	0.027	-0.016
5	-0.014	-0.011	-0.012	-0.015	-0.015	-0.012	-0.013
6	0.075	0.069	0.072	0.068	0.068	0.070	0.071
7	0.034	0.035	0.037	0.035	0.035	0.034	0.037
8	0.029	0.029	0.027	0.026	0.026	0.028	0.027
9	0.003	0.003	0.002	0.003	0.003	0.003	0.002
10	0.037	0.036	0.036	0.034	0.034	0.035	0.035
11	0.575	0.574	0.575	0.574	0.574	0.574	0.574
12	-0.499	-0.499	-0.499	-0.499	-0.499	-0.499	-0.499
13	-0.146	-0.147	-0.147	-0.147	-0.147	-0.147	-0.147
14	-0.046	-0.033	0.003	-0.041	-0.017	-0.037	0.001
15	-0.072	-0.059	-0.019	-0.066	-0.045	-0.063	-0.019
M	1.1328	1.1333	1.0652	2.1269	1.757	1.1331	1.066

Table S2B

R	S_0	S_1	T_1	S_2
1-2	1.385	1.366	1.368	1.383
2-3	1.398	1.421	1.422	1.400
3-4	1.414	1.447	1.453	1.430
4-5	1.396	1.417	1.418	1.410
5-6	1.394	1.376	1.380	1.386
6-7	1.484	1.480	1.480	1.483
7-8	1.397	1.398	1.398	1.397
8-9	1.393	1.392	1.392	1.393
9-10	1.391	1.392	1.392	1.391
9-11	1.487	1.487	1.487	1.487
11-12	1.212	1.212	1.212	1.212
11-13	1.339	1.339	1.339	1.340
4-14	1.428	1.385	1.387	1.403
14-15	1.209	1.229	1.232	1.224

Table S2. (**A**) Mulliken atomic charges (in a.u.) of the different carbon atoms in the considered electronic states of isoT12H_6. The charge of hydrogen atoms bonded to a given carbon atom is included. For the numeration of atoms, see Scheme S2B. FC correspond to the Franck-Condon level. (**B**) Internuclear C–C distances (Å) in the selected electronic states of isoT12H_6.

7. Optical properties of the compounds

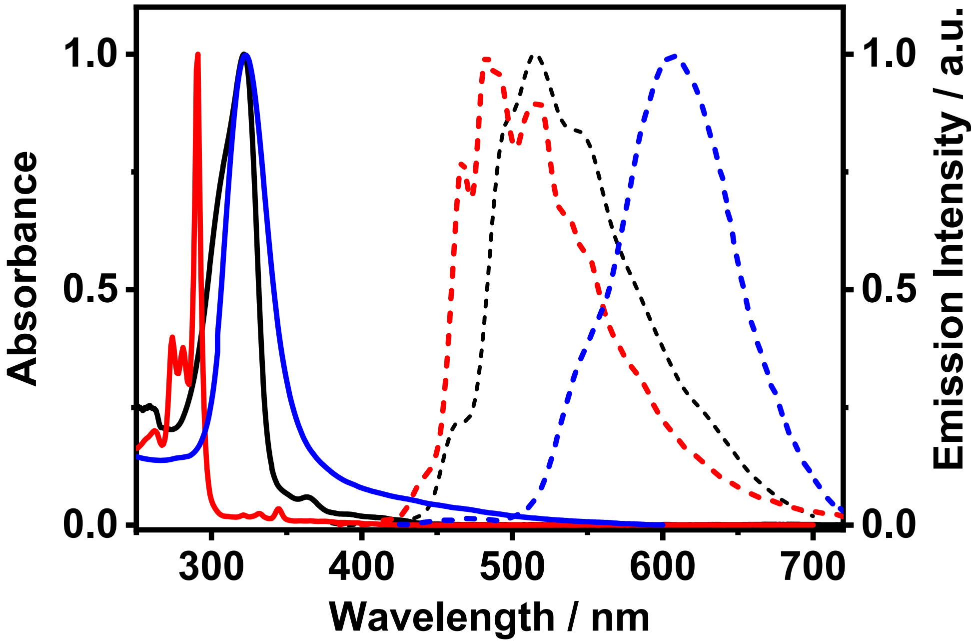

Figure S13. UV-visible absorption (solid lines) and emission spectra (dashed lines) of isoT12H$_6$ (black), Nu-T12 (red) and T12-COOH (blue) in DMF solutions. The excitation wavelength for the emission spectra is 370 nm.

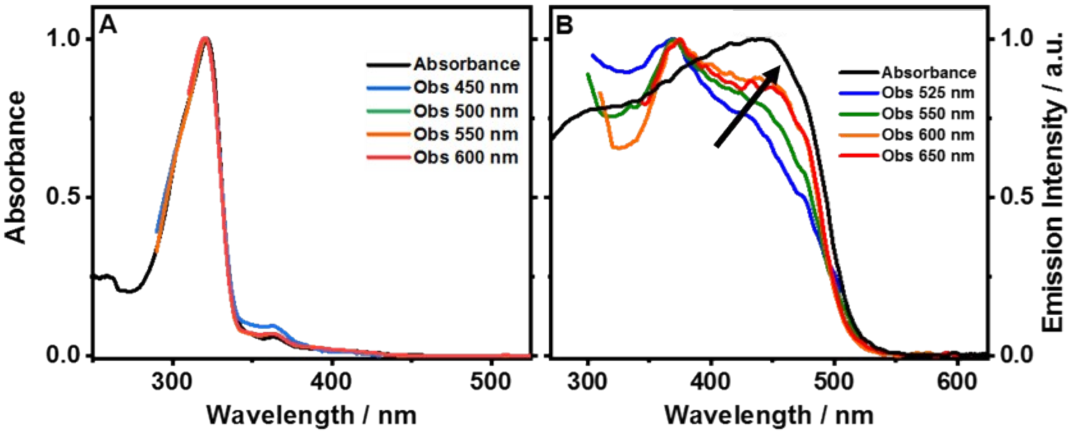

Figure S14. Normalized UV-visible absorption and excitation spectra of isoT12H$_6$ in A) DMF solution and B) solid state. The observation wavelengths for the excitation spectra are as indicated.

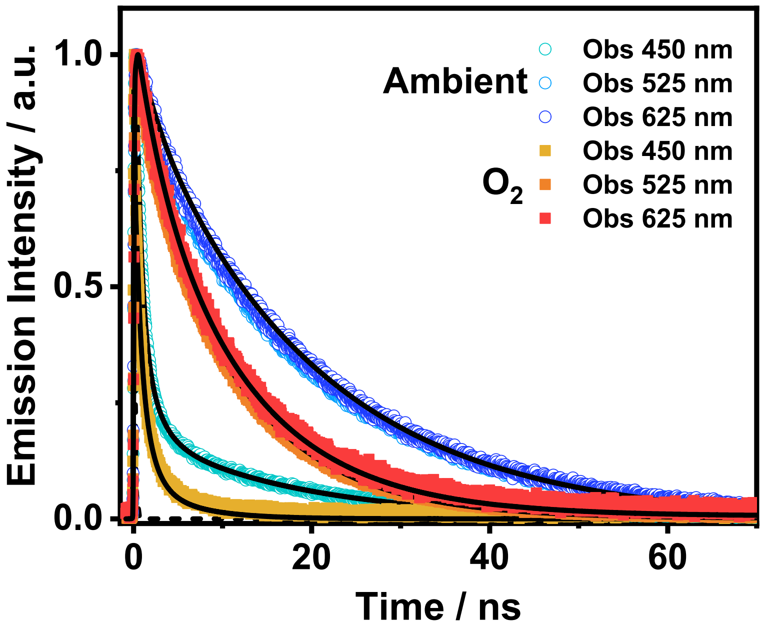

Figure S15. Normalized magic-angle emission decays of isoT12H$_6$ in DMF solution in ambient (empty circles) and oxygen (solid squares) atmospheres, upon excitation at 371 nm. The solid lines are from the best global fit using a multiexponential function. The dashed line is the IRF of the setup.

Atmosphere	λ_{obs} (nm)	τ_1 (ps) ±100 ps	a_1	c_1	τ_2 (ns) ±0.1 ns	a_2	c_2	τ_3 (ns) ±0.3 ns	a_3	c_3
Ambient	450	570	43	7	1.44	43	19	20.6	14	74
	525		-	-		12	1		88	99
	625		-	-		6	1		94	99
O_2	450	570	44	16	1.49	54	59	10.6	2	25
	525		-	-		20	4		80	96
	625		-	-		19	4		81	96

Table S3. Values of time constants (τ_i), normalized (to 100) pre-exponential factors (a_i) and contributions ($c_i=(\tau_i \times a_i)/\sum(\tau_i \times a_i)$) in the signal obtained from a global multiexponential fit of isoT12H$_6$ in DMF solution under ambient and oxygen atmospheres. The excitation wavelength was 371 nm, and the observation wavelengths are as indicated.

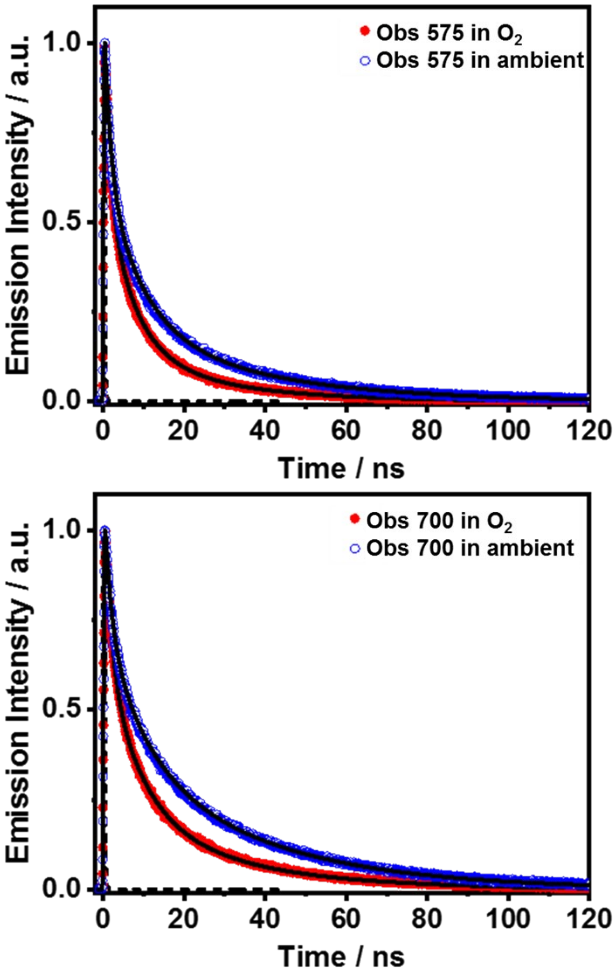

Figure S16. Normalized magic-angle emission decays of isoT12H_6 in solid state in ambient (blue open circles) and oxygen (red solid circles) atmospheres, upon excitation at 371 nm and observation at A) 575 nm and B) 700 nm. The solid lines are from the best global fit using a multiexponential function. The dashed line is the IRF of the setup.

Atmosphere	**λ_{obs} (nm)**	**τ_1 (ns) ±0.1 ns**	**a_1**	**c_1**	**τ_2 (ns) ±0.2 ns**	**a_2**	**c_2**	**τ_3 (ns) ±0.4 ns**	**a_3**	**c_3**
Ambient	575	1.5	41	6	8.9	39	31	34.0	20	63
	700		31	3		33	17		37	80
O_2	575	1.5	54	14	8.7	36	45	28.0	10	41
	700		41	7		40	34		19	55

Table S4. Values of time constants (τ_i), normalized (to 100) pre-exponential factors (a_i) and contributions ($c_i=(\tau_i \times a_i)/\sum(\tau_i \times a_i)$) in the signal obtained from a global multiexponential fit of isoT12H_6 in solid sta.te under ambient and oxygen atmospheres. The excitation was 371 nm and the observation wavelengths are as indicated.

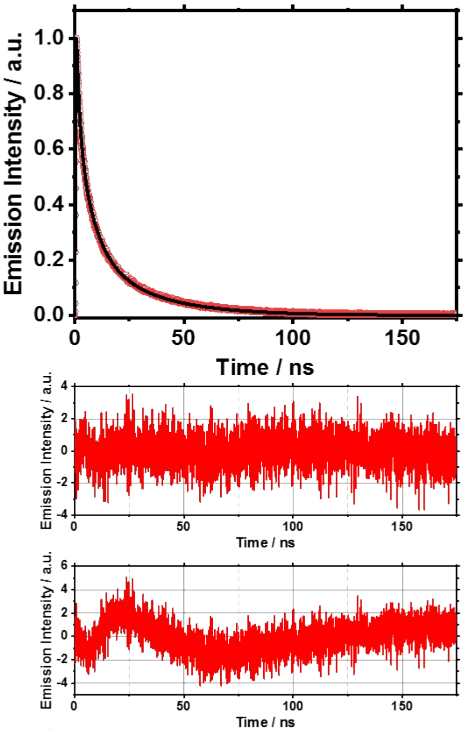

1.5 ns, 8.7 ns y 28 ns, Chi=0.98

1.5 ns, 8.7 ns y 33 ns, Chi=1.67

Figure S17. Normalized magic-angle emission decays of isoT12H$_6$ in solid state under oxygen atmosphere, upon excitation at 371 nm, and observing at 700 nm. The solid line is from the best global fit using a multiexponential function. The residual distribution corresponds to the indicated time constants used in the fits.

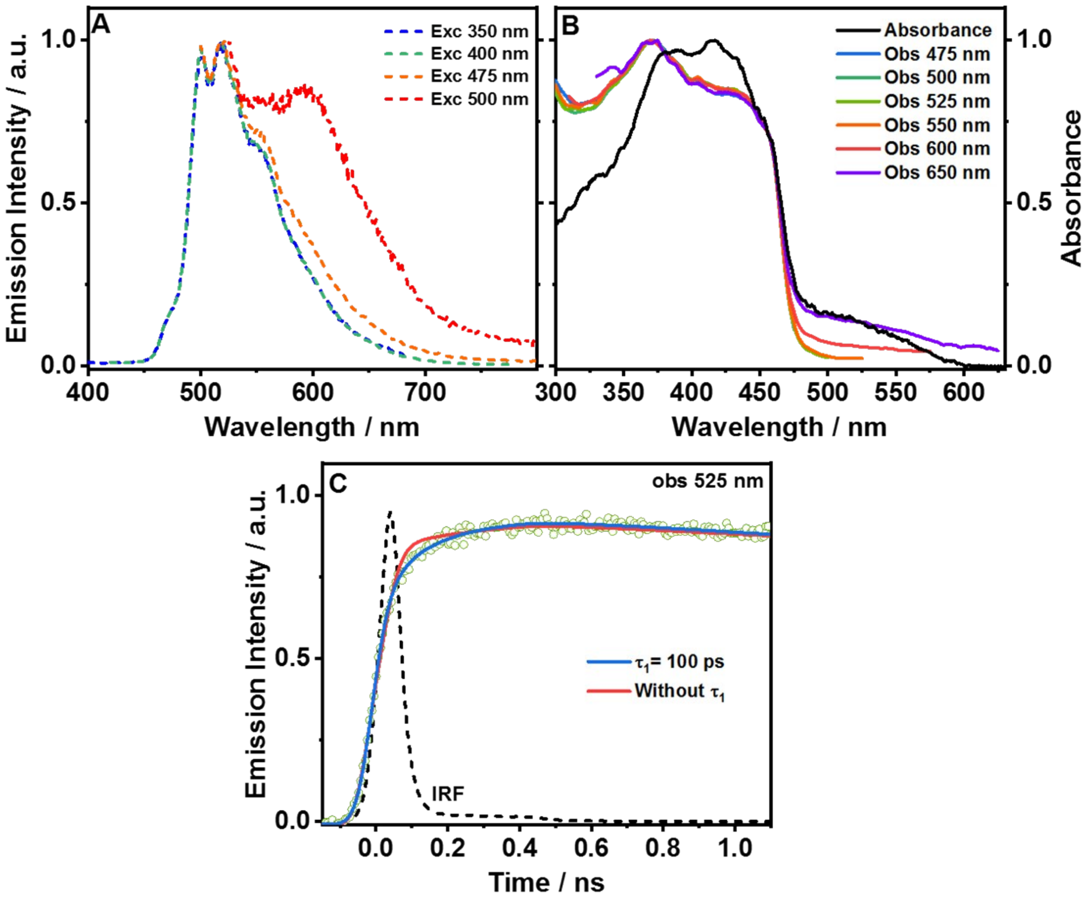

Figure S18. A) Emission spectra and B) UV-visible absorption and excitation spectra of the ensemble MOF-isoT12(Zn) in solid state at different excitation and observation wavelengths. C) Representative emission decay in a short time window of MOF-isoT12(Zn) upon excitation at 371 nm. The solid lines are from the two fits (without and with rising component) using a multiexponential function.

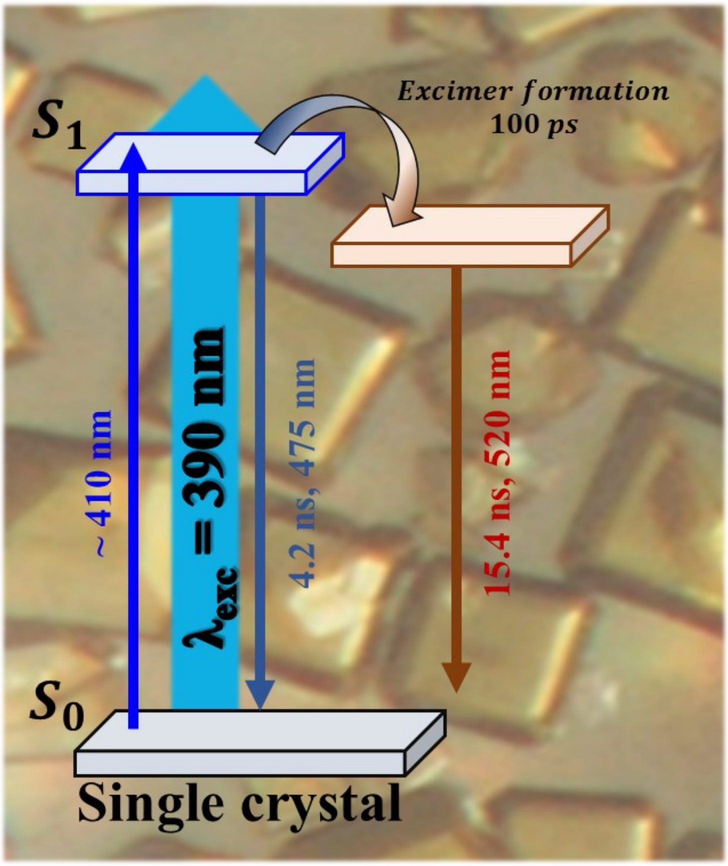

Scheme S3. Photophysical diagram (not to scale) showing the time constants and spectral ranges along with the electronic transitions, involved processes and emissive states in a single crystal of MOF-isoT12(Zn) in solid state.

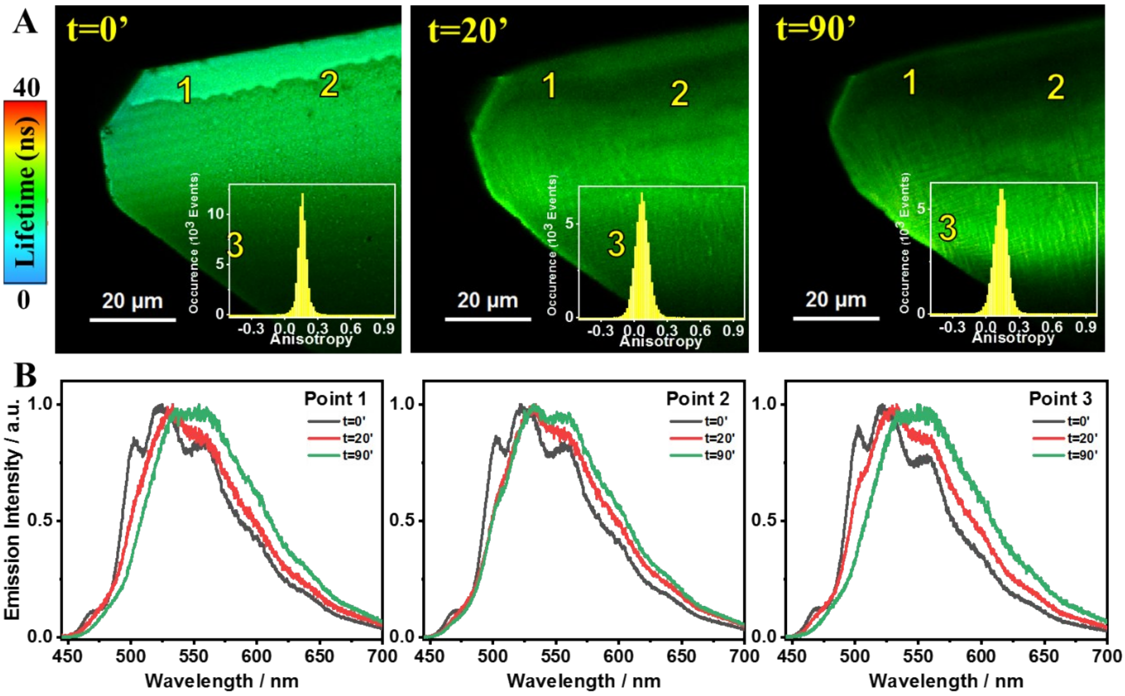

Figure S19. A) FLIM images of MOF-isoT12(Zn) crystals in DCM after different exposure times to air. The insets show the histogram of the emission anisotropy of the related crystals. B) Emission spectra at selected points (as indicated in Fig. S19A) of the related crystals and at different times of exposure to ambient conditions. The excitation wavelength was 390 nm.

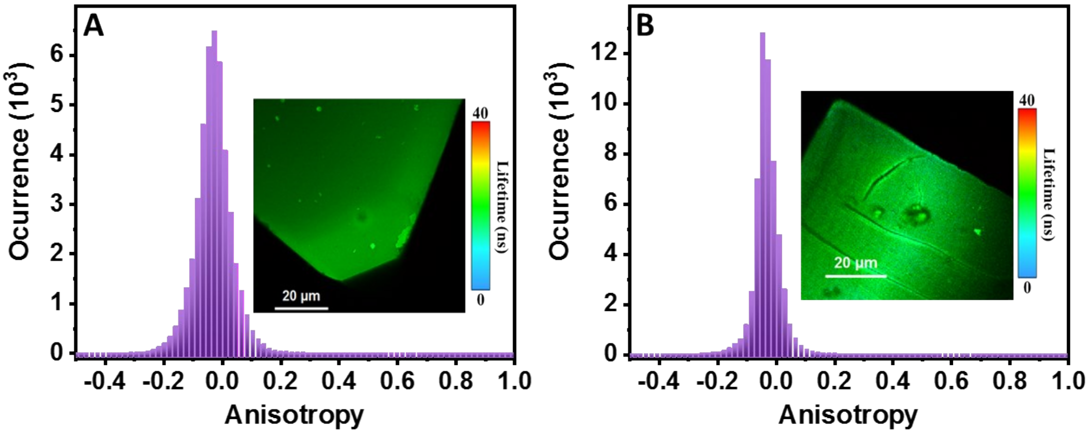

Figure S20. Histogram of the emission anisotropy of MOF-isoT12(Zn) A) neat crystal and B) sonicated for 15 minutes in DCM, upon excitation at 390 nm. The insets show the corresponding FLIM images.

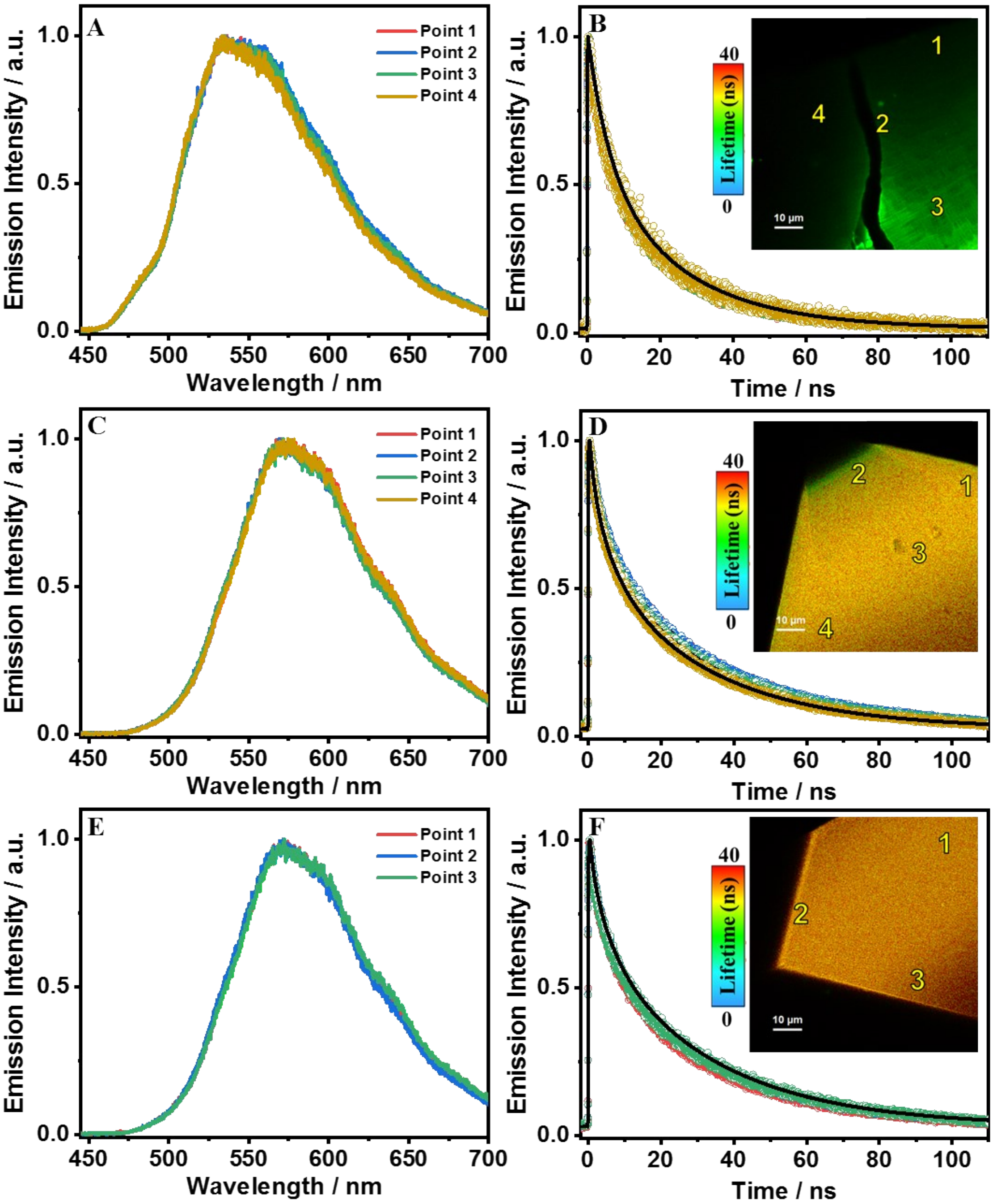

Figure S21. Emission spectra at selected points (indicated in the FLIM images) of MOF-isoT12(Zn) crystals after A) 2 days in vacuum, C) and E) 2 days in water-enriched atmosphere. B), D) and F) Emission decays of the related crystals. The insets show the FLIM images of the related crystals. The excitation wavelength was 390 nm.

A)

Point	**τ_1 (ns)**	**a_1**	**τ_2 (ns)**	**a_2**
1	5.4	41	23.0	5951 53 58
2	5.3	49	23.0	
3	5.3	47	22.0	
4	5.5	42	23.0	
Average	5.4	45	23.0	55

B)

Point	**τ_1 (ns)**	**a_1**	**τ_2 (ns)**	**a_2**	**τ_3 (ns)**	**a_3**
1	1.5	14	6.4	24	32.0	62
2	1.5	13	6.3	25	32.0	62
3	1.5	16	6.5	26	32.0	58
4	1.5	15	6.3	27	32.0	58
Average	1.5	15	6.4	25	32.0	60

C)

Point	**τ_1 (ns)**	**a_1**	**τ_2 (ns)**	**a_2**	**τ_3 (ns)**	**a_3**
1	1.1	15	6.0	28	31.0	58
2	1.2	12	5.9	26	32.0	62
3	1.3	12	5.9	25	32.0	63
Average	1.2	13	5.9	26	32.0	61

Table S5. Values of time constants (τ_i) and normalized (to 100) pre-exponential factors (a_i) obtained from the fit of the emission decays of the different points of the MOF-isoT12(Zn) crystal after A) 2 days in vacuum, B) and C) 2 days in water-enriched atmosphere. The fluorescence lifetime images of the related crystals are shown in Figure S20.

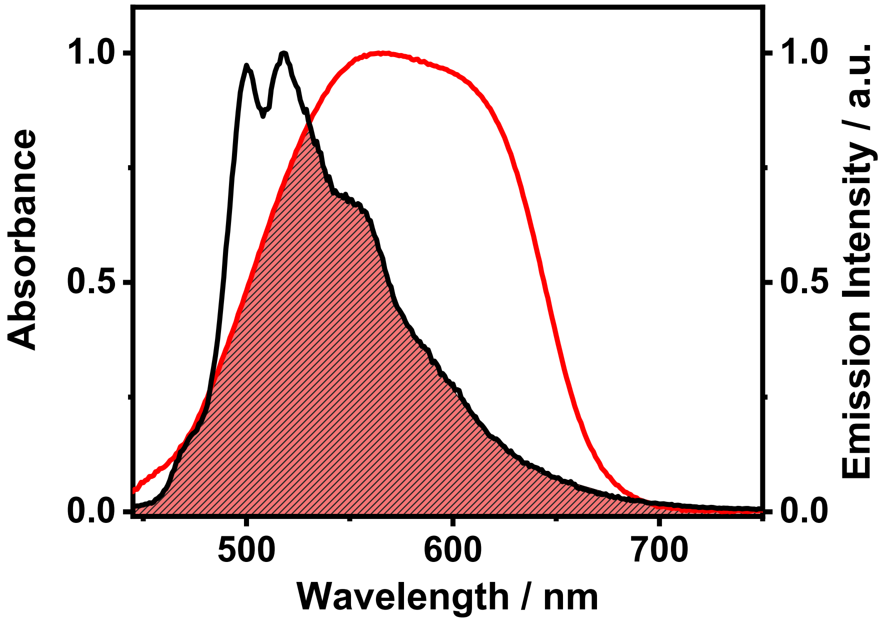

Figure S22. Normalized steady-state UV-visible absorption of NR on silica mesostructured (red) and emission spectra, exciting at 400 nm of MOF-isoT12(Zn) (black). The shaded area indicates the spectral overlap.

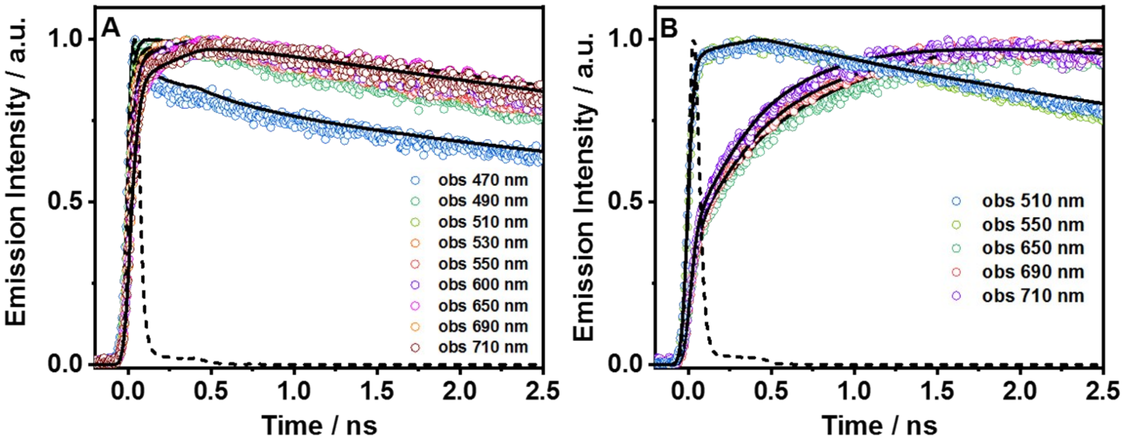

Figure S23. Normalized mission decays in a short time window of NR@MOF-isoT12(Zn) composites, A) $2.5x10^{-6}$ M (M1) and B) $2.5x10^{-5}$ M (M2), upon excitation at 371 nm. The solid lines are from the best fits using a multiexponential function, and IRF (dashed line) is the instrumental response function.

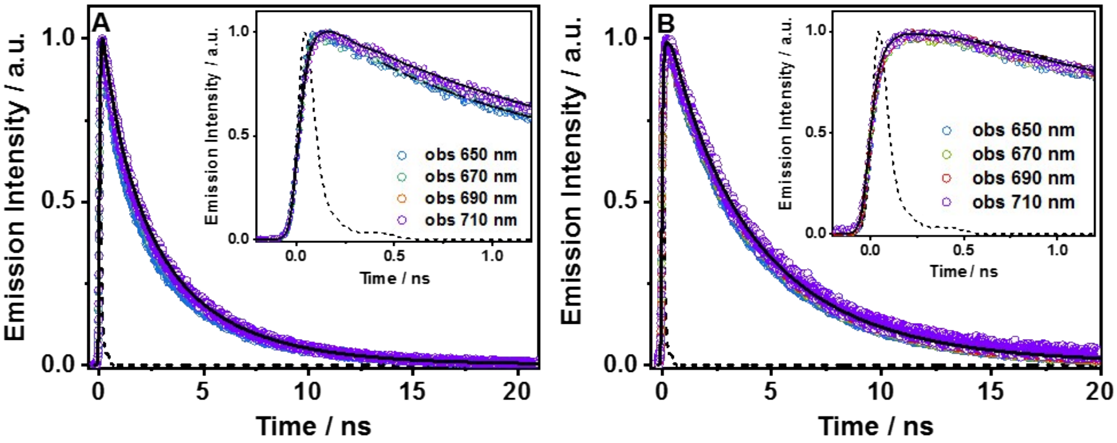

Figure S24. Magic-angle emission decays of NR@MOF-isoT12(Zn) composites, A) 2.5x10^{-6} M (M1) and B) 2.5x10^{-5} M (M2), upon excitation at 635 nm. The solid lines are from the best fits using a multiexponential function, and IRF (dashed line) is the instrumental response function. The insets show the same decays in a short time window.

Sample	λ_{obs} (nm)	τ_1 (ps) ±50 ps	a_1	c_1	τ_2 (ns) ±0.1 ns	a_2	c_2	τ_3 (ns) ±0.2 ns	a_3	c_3
M1	**650**	207	29	3	1.5	33	22	4.1	38	75
	670		28	3		32	21		40	76
	690		27	2		32	22		41	76
	710		26	2		32	22		41	76
M2	**650**	-	-	-	1.7	22	8	4.2	78	92
	670					20	7		80	93
	690					20	7		80	93
	710					19	7		81	93

Table S6. Values of time constants (τ_i), normalized (to 100) pre-exponential factors (a_i) and contributions ($c_i=(\tau_i\times a_i)/\sum(\tau_i\times a_i)$) in the signal obtained from a global multiexponential fit of NR@MOF-isoT12(Zn) composites. The excitation wavelength was 635 nm. The observation wavelengths are as indicated.

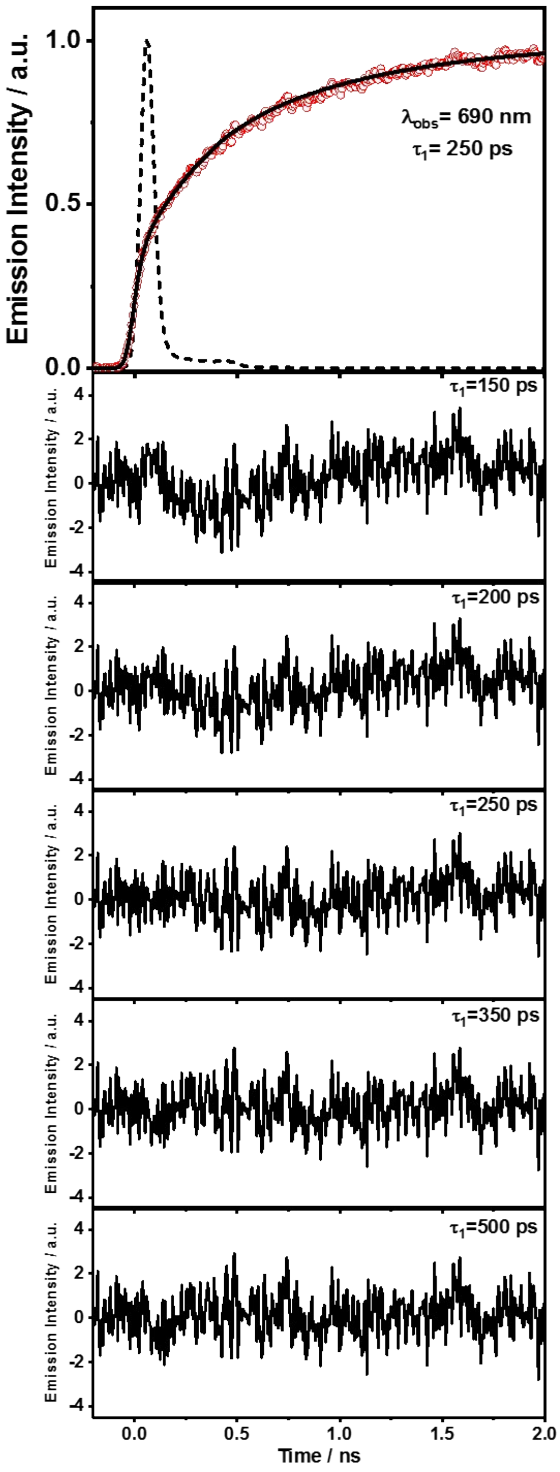

Figure S25. Representative emission decay in a short time window of NR@MOF-isoT12(Zn) ($2.5\mathrm{x}10^{-5}$ M (M2)) upon excitation at 371 nm and observing at 690 nm. The solid lines are from the best-fit using a multiexponential function, and IRF (dashed line) is the instrumental response function. The residual distributions correspond to different values of the short rising component used in the fits.

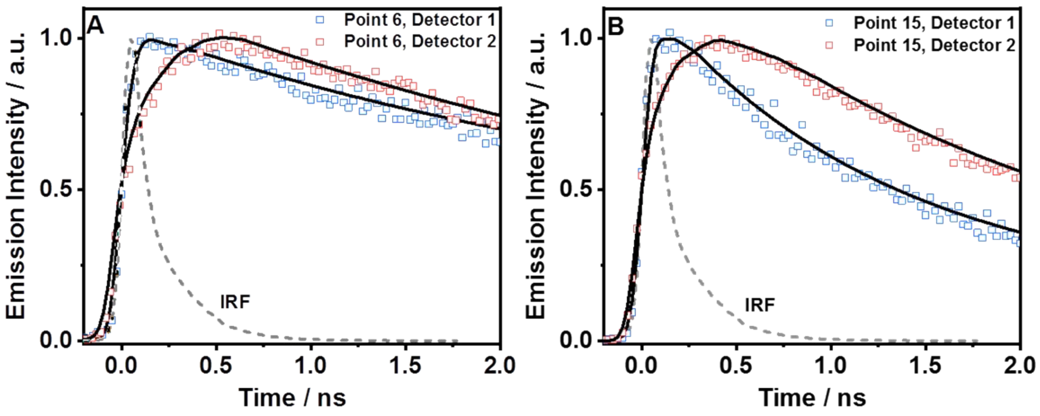

Figure S26. Comparison of the emission decays corresponding to A) point 6 and B) point 15 of the NR@MOF-isoT12(Zn) of Figure 8 in the main text, collected at detector 1 and detector 2, using two different filters of transmission.

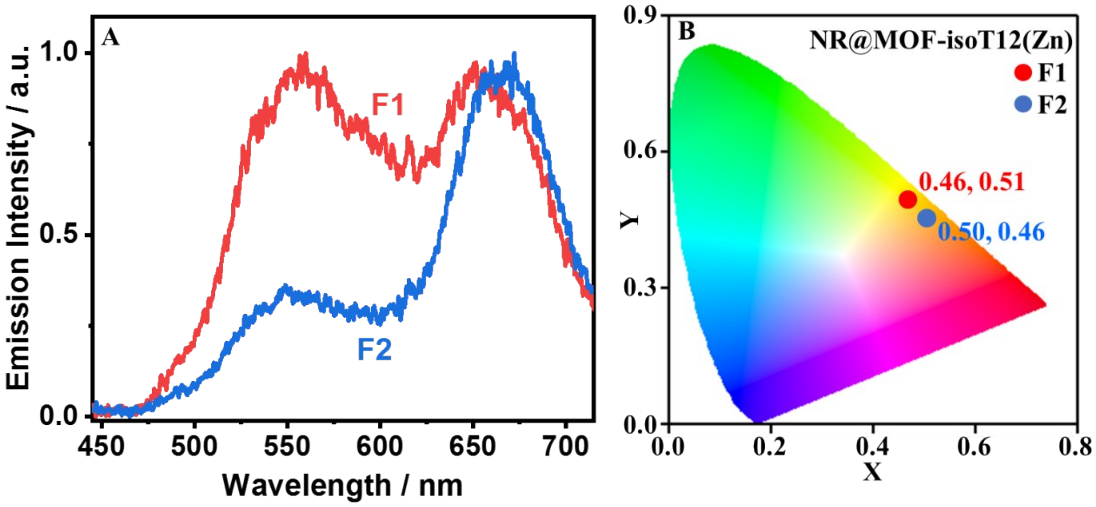

Figure S27. A) Representative emission spectra of the two different families (F1, red and F2, blue) of the composites of NR@MOF-isoT12(Zn) of Figure 8 in the main text. B) Commission International De I'Eclairage coordinates of the two emission spectra of NR@MOF-isoT12(Zn) composite.

Point	Detector	τ_1 (ns)	a_1	τ_2 (ns)	a_2
1	1	3.4	58	22.0	42
	2	3.4	84	18.0	16
2	1	2.8	57	21.0	43
	2	3.9	85	18.0	15
3	1	2.7	64	22.0	36
	2	3.8	84	17.0	16
4	1	3.1	52	22.0	48
	2	4.0	82	21.0	18
5	1	3.2	57	22.0	43
	2	3.6	84	19.0	16
6	1	3.2	61	23.0	39
	2	3.6	85	18.0	15
7	1	2.5	76	10.0	24
	2	2.7	87	9.8	13
8	1	1.4	88	9.8	12
	2	2.1	89	7.5	11
9	1	1.4	77	9.8	23
	2	2.7	89	9.2	14
10	1	1.2	80	7.1	20
	2	2.1	86	7.2	14
11	1	1.8	79	9.8	21
	2	2.8	86	9.3	14
12	1	1.4	81	8.0	19
	2	2.2	87	7.8	13
13	1	2.4	67	10.0	33
	2	3.1	85	9.5	15
14	1	1.6	81	8.2	19
	2	2.3	85	7.9	15
15	1	1.0	80	9.0	20
	2	2.1	84	7.5	16

Table S7. Values of time constants (τ_i) and normalized (to 100) pre-exponential factors (a_i) obtained from the fit of the emission decays of the different points of the NR@MOF-isoT12(Zn) composites.

REFERENCES

1. Rigaku, *CrystalStructure, Rigaku Corporation, Version 4.3, Tokyo, Japan*, 2018.
2. G. Sheldrick, *Acta Crystallogr. Sect. A*, 2015, **71**, 3-8.
3. G. Sheldrick, *Acta Crystallogr. Sect. A*, 2008, **64**, 112-122.
4. J. A. Organero, L. Tormo and A. Douhal, *Chem. Phys. Lett.*, 2002, **363**, 409-414.
5. J. Schaffer, A. Volkmer, C. Eggeling, V. Subramaniam, G. Striker and C. A. M. Seidel, *J. Phys. Chem. A*, 1999, **103**, 331-336.
6. V. Buschmann, A. Bleckmann, A. Bülter, B. Krämer, J. Nikolaus, R. Schwarzer, T. Korte, J. Ziomkowska, A. Herrmann and F. Koberling, *PicoQuant*.
7. N. C. Handy, *Mol. Phys.*, 2004, **102**, 2399-2409.
8. P. C. Hariharan and J. A. Pople, *Theor. Chim. Acta*, 1973, **28**, 213-222.
9. M. M. Francl, W. J. Pietro, W. J. Hehre, J. S. Binkley, M. S. Gordon, D. J. DeFrees and J. A. Pople, *J. Chem. Phys.*, 1982, **77**, 3654-3665.
10. S. Miertuš, E. Scrocco and J. Tomasi, *Chem. Phys.*, 1981, **55**, 117-129.
11. R. Improta, V. Barone, G. Scalmani and M. J. Frisch, *J. Chem. Phys.*, 2006, **125**, 054103.
12. M. J. Frisch, G. W. Trucks, H. B. Schlegel, G. E. Scuseria, M. A. Robb, J. R. Cheeseman, G. Scalmani, V. Barone, B. Mennucci, G. A. Petersson, H. Nakatsuji, M. Caricato, X. Li, H. P. Hratchian, A. F. Izmaylov, J. Bloino, G. Zheng, J. L. Sonnenberg, M. Hada, M. Ehara, K. Toyota, R. Fukuda, J. Hasegawa, M. Ishida, T. Nakajima, Y. Honda, O. Kitao, H. Nakai, T. Vreven, J. A. Montgomery, J. E. Peralta, F. Ogliaro, M. Bearpark, J. J. Heyd, E. Brothers, K. N. Kudin, V. N. Staroverov, R. Kobayashi, J. Normand, K. Raghavachari, A. Rendell, J. C. Burant, S. S. Iyengar, J. Tomasi, M. Cossi, N. Rega, J. M. Millam, M. Klene, J. E. Knox, J. B. Cross, V. Bakken, C. Adamo, J. Jaramillo, R. Gomperts, R. E. Stratmann, O. Yazyev, A. J. Austin, R. Cammi, C. Pomelli, J. W. Ochterski, R. L. Martin, K. Morokuma, V. G. Zakrzewski, G. A. Voth, P. Salvador, J. J. Dannenberg, S. Dapprich, A. D. Daniels, Farkas, J. B. Foresman, J. V. Ortiz, J. Cioslowski and D. J. Fox, *Gaussian 09, (Revision D.01). Gaussian, Inc., Wallingford CT*, 2009.